Ab initio molecular dynamics studies of the photodissociation of formaldehyde, $H_2CO \rightarrow H_2+CO$: Direct classical trajectory calculations by MP2 and density functional theory

Xiaosong Li, John M. Millam, and H. Bernhard Schlegel
Department of Chemistry, Wayne State University, Detroit, Michigan 48202

(Received 14 July 2000; accepted 18 September 2000)

The dynamics of $H_2CO \rightarrow H_2+CO$ photodissociation have been studied by classical trajectory calculations at the MP2/6-311G(d,p), B3LYP/6-311G(d,p), and VSXC/6-311G(d,p) levels of theory. The trajectories were calculated directly from the electronic structure computations without first fitting a global potential energy surface. A Hessian based method with updating was used to integrate the trajectories. The translational energy distribution of the products is in better agreement with experiment than the previous Hartree–Fock direct trajectory calculations, since the MP2 and density functional methods reproduce the barrier height better. The MP2 and density functional calculations give very good descriptions of the product rotational state distributions and the CO vibrational state populations. The MP2 method yields a very good representation of the H_2 vibrational state populations, whereas the density functional methods give too little H_2 vibrational excitation and Hartree–Fock produces too much. This can be attributed to the difference in the potential energy release that accompanies the formation of the H_2 bond. © *2000 American Institute of Physics.* [S0021-9606(00)01646-9]

I. INTRODUCTION

The photodissociation of formaldehyde has been studied extensively, both experimentally[1–13] and theoretically.[14–29] Excitation of formaldehyde to the S_1 state is followed by rapid internal conversion to the S_0 state with a high degree of vibrational excitation. At higher photolysis energies, dissociation to hydrogen atom and formyl radical is possible, $H_2CO \rightarrow H+HCO$. Below this threshold, dissociation proceeds to hydrogen molecule and carbon monoxide, $H_2CO \rightarrow H_2+CO$. A series of elegant experiments[1–13] on this latter channel has yielded a very detailed description of the product energy distributions. Consequently, this reaction serves as an excellent test case for theoretical studies of molecular dynamics.[23–29]

The transition state for $H_2CO \rightarrow H_2+CO$ is well characterized theoretically,[14–22] and best calculations[22] predict a barrier 2–3 kcal/mol higher than the experimental estimate.[9] Several classical trajectory studies have been carried out on this reaction.[26–29] Miller and co-workers[27] have calculated trajectories on global potential energy surfaces using an empirical valence bond (EVB) approximation fitted to MP2/DZP and CCSD/TZ2P energies. Chen, Hase, and Schlegel[28] performed *ab initio* direct trajectory calculations at the Hartree–Fock level, in which the potential energy surface is computed ''on the fly'' rather than fitted to an approximate, analytic form. Peslherbe and Hase[29] tested the suitability of semiempirical methods for direct trajectory calculations, using AM1, PM3, and NDDO methods with specific reaction parameters.

The primary bottleneck in conventional trajectory calculations is the generation of a suitably accurate potential energy surface.[30] Direct classical trajectory calculations circumvent this bottleneck by using electronic structure methods to compute the necessary energies, gradients, and Hessians as they are needed.[31–33] These methods are becoming more and more practical with the rapid increases in computational speed and affordability. In the present paper, we have extended our previous work at the Hartree–Fock level[28] by calculating direct classical trajectories for the photodissociation of formaldehyde using second order Moller–Plesset perturbation theory (MP2) and density functional theory (DFT). In particular, classical trajectories have been computed for $H_2CO \rightarrow H_2+CO$ with the MP2,[34,35] B3LYP,[36–38] and VSXC[39,40] methods using the 6-311G(d,p) basis set.[41] MP2 is the simplest *ab initio* method that treats electron correlation; B3LYP has been used extensively and gives good energies and structures; VSXC is a recent functional that also gives good energetics but does not require the HF exchange. Other functionals that give reasonable energetics for formaldehyde dissociation include B3PW91[42] and MPW1PW91.[43]

II. METHOD

As in earlier studies,[27–29] the initial conditions for the trajectory calculations have been chosen to simulate the experimental photolysis of formaldehyde at 29 500 cm^{-1}. As in previous studies, trajectories were started at the transition state, with 5.1 kcal/mol kinetic energy in reaction coordinate, corresponding to the difference between the photolysis energy and the estimated barrier height. Zero point energy was added to the remaining vibrational coordinates, with a suitable random distribution of initial vibrational coordinates and momenta. The total angular momentum was set to zero. For each level of theory [MP2/6-311G(d,p),B3LYP/

TABLE I. Optimized geometries for the transition state for $H_2CO \rightarrow H_2+CO$ (Å and degrees).

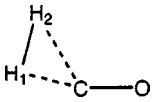

Level	C–O	H–H	C–H_1	C–H_2	O–C–H_2
HF/6-31G(d,p)	1.141	1.255	1.095	1.649	114.1
MP2/6-311G(d,p)	1.170	1.298	1.093	1.670	113.4
B3LYP/6-311G(d,p)	1.159	1.321	1.091	1.701	113.6
B3PW91/6-311G(d,p)	1.160	1.298	1.095	1.675	113.0
MP1PW91/6-311G(d,p)	1.157	1.286	1.095	1.664	112.9
VSXC/6-311G(d,p)	1.167	1.336	1.088	1.698	113.4
QCISD/6-311G(d,p)	1.169	1.307	1.094	1.664	112.1
CCSD/TZ2P[a]	1.163	1.307	1.093	1.661	111.3
CCSD(T)/aVTZ[b]	1.173	1.326	1.096		

[a]Reference 20.
[b]Reference 22.

6-311G(d,p), and VSXC/6-311G(d,p)], 200 trajectories were integrated using our Hessian based predictor-corrector method.[44,45] The Hessian was updated for 5 steps before being recalculated analytically. A step size of 0.25 $amu^{1/2}$ bohr was used for all of the calculations, and the trajectories were stopped when the products were ≈13 bohr apart or the gradient of the potential between product molecules was less than 5×10^{-7} hartree/bohr. The average time for a trajectory was 35–40 fs, and total energy was conserved to 10^{-7} hartree. Total angular momentum was conserved to better than $10^{-8}\hbar$ since projection methods were used to remove the overall angular forces. The mass-weighted steepest descent reaction paths were calculated using the method of Gonzalez and Schlegel.[46,47] The calculations were carried out with the development version of the Gaussian series of programs.[48] Typical MP2, B3LYP, and VSXC trajectories ran for 83, 160, and 420 min, respectively, on a 450 MHz Pentium III.

III. RESULTS AND DISCUSSION

The calculated geometries for the transition states are shown in Table I. The H–H bond lengths at the B3LYP/6-311G(d,p) and VSXC/6-311G(d,p) levels of theory are in good agreement with the best available values;[22] but are somewhat too short at MP2/6-311G(d,p), QCISD/6-311G(d,p), and CCSD/TZ2P.[20] The calculated energetics are summarized in Table II. The G2,[49–51] CBS-APNO,[52] and CCSD(T)/aV5Z+corr (Ref. 22) values are probably the most accurate, with estimated errors of 1.5, 0.5, and 0.3 kcal/mol, respectively, and agree very well with the experimental heat of reaction. The barrier heights at the G2 and CBS-APNO levels (81.6 and 81.1 kcal/mol, respectively) are in excellent agreement with the best available calculations [81.9 kcal/mol,CCSD(T)/aV5Z +corrections for core-valence correlation and relativistic effects],[22] as well as earlier calculations (81.4 kcal/mol, CCSDT-1/TZ2P).[20] All of these high level theoretical values are 2–3 kcal/mol above the experimental estimate of 79.2 ±0.8 kcal/mol.[9] The MP2 and DFT barrier heights are in much better agreement with the high level values than the HF/3-21G and HF/6-31G(d,p) calculations used in our previous direct dynamics study.[28] The barrier for the reverse reaction corresponds to the potential energy release; again, the present calculations are in better agreement with experiment than the Hartree–Fock calculations.

The potential energy profiles along the intrinsic reaction coordinate (mass-weighted steepest descent path) are shown in Fig. 1. The total energy release from the transition state to the products is too large by ≈25 kcal/mol at the Hartree–Fock level, ≈10 kcal/mol too high at MP2, 2–4 and 7–9 kcal/mol too low at B3LYP and VSXC, respectively. The change in the H_2 bond length is 80%–85% complete (0.8–0.9 Å) by $s=1.0\,amu^{1/2}$ bohr in the path length, which corresponds to C–H bond lengths of 1.3–1.4 Å and 1.8–1.9 Å. Plots of the bond lengths vs reaction coordinate are nearly superimposable up to this point. However, only ≈50% of the potential energy has been released by $s=1.0\,amu^{1/2}$ bohr.

The harmonic vibrational frequencies for the transition state are compared in Table III. On average, the B3LYP and VSXC frequencies are a bit lower than the MP2 frequencies, but the MP2 and DFT values are better than HF when compared with the CCSD and CCSD(T) results.[20,22] The components of the transition vector are very similar for the HF, MP2, and DFT calculations. Figure 2 shows the variations of

TABLE II. Heat of reaction and barrier height for $H_2CO \rightarrow H_2+CO$ (in kcal/mol).

Level	ΔH_0^0	Forward $\Delta H_0^{\ddagger}$	Reverse $\Delta H_0^{\ddagger}$
HF/6-31G(d,p)	−7.7	98.8	106.5
MP2/6-311G(d,p)	−7.3	84.8	92.1
B3LYP/6-311G(d,p)	−0.5	79.3	79.8
B3PW91/6-311G(d,p)	2.3	79.9	77.6
MP1PW91/6-311G(d,p)	3.4	81.3	77.9
VSXC/6-311G(d,p)	1.4	76.1	74.7
CCSDT-1/TZ2P[a]	−4.5	81.4	85.9
G2	−3.1	81.6	84.7
CBS-APNO	−2.1	81.1	83.2
CCSD(T)/aV5Z+corr[b]	−1.6	81.9	83.5
Experiment[c]	−2.2±0.14	79.2±0.8	81.4±0.9

[a]Reference 20.
[b]Reference 22.
[c]Reference 9.

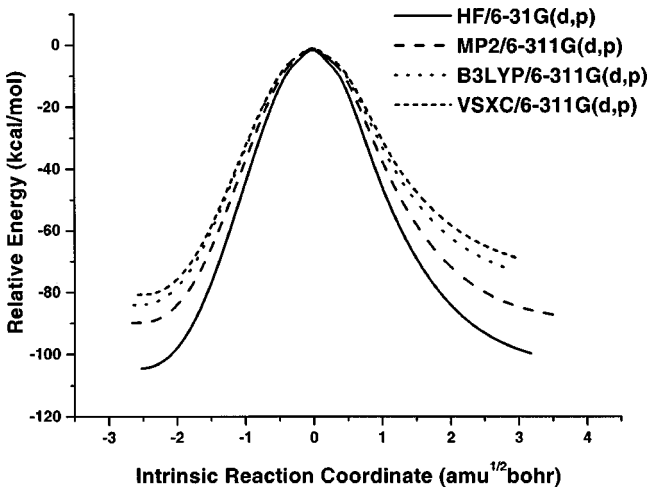

FIG. 1. Potential energy profiles along the reaction path at the HF/6-31G(d,p), MP2/6-311G(d,p), B3LYP/6-311G(d,p), and VSXC/6-311G(d,p) levels of theory.

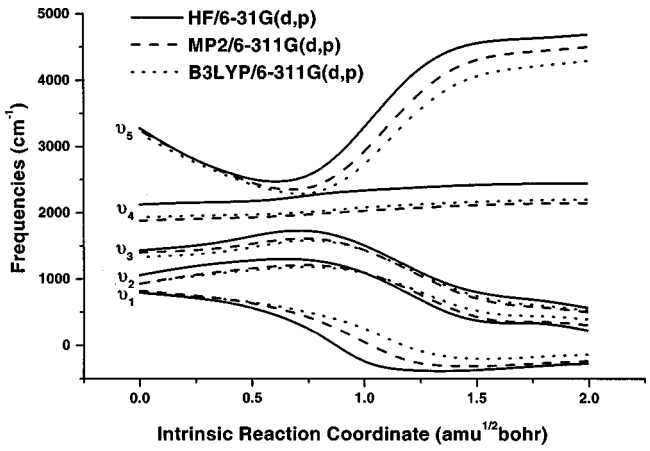

FIG. 2. Projected vibrational frequencies along the reaction path at the HF/6-31G(d,p), MP2/6-311G(d,p), and B3LYP/6-311G(d,p) levels of theory.

the projected frequencies along the reaction path. Again, these are very similar in the critical range of $s = 0-1.0\,\mathrm{amu}^{1/2}\,\mathrm{bohr}$ where most of the important geometrical changes occur.

The total product translational energy distributions are shown in Fig. 3. The averages of the MP2, B3LYP, and VSXC distributions are 68, 60, and 55 kcal/mol. This corresponds to 69%–71% of the available energy, compared to 76%–82% of the available energy for trajectories with semiempirical methods.[29] The experimental value is 55 kcal/mol[2] (65%) and 60 kcal/mol (70%) has been obtained from calculations on the EVB/CCSD surface.[27] The present results are a significant improvement over the HF/3-21G and HF/6-31G(d,p) data[28] (75 and 80 kcal/mol, respectively). The Hartree–Fock calculations overestimate the energy released in going to products by ≈25 kcal/mol and most of the excess energy stays in the translational modes. By comparison, the potential energy released computed by MP2, B3LYP, and VSXC differ from experiment by ≈10, −2, and −7 kcal/mol. The average translational energy calculated at the MP2 and DFT levels does not depend on the CO vibrational quantum number, but decreases by ≈8 kcal/mol for each increment in the H_2 vibrational quantum number, similar to our previous calculations at the Hartree–Fock level.

The average outgoing impact parameters are 0.85, 0.95, 0.98, and 1.06 Å for HF/6-31G(d,p),MP2/6-311G(d,p), B3LYP/6-311G(d,p), and VSXC/6-311G(d,p), respec-

TABLE III. Harmonic vibrational frequencies and transition vector for the transition state of $H_2CO \rightarrow H_2+CO$.

Level	HF[a]	MP2[b]	B3LYP[b]	VSXC[b]	CCSD[c]	CCSD(T)[d]
Harmonic vibrational frequencies (cm^{-1})						
ν_1	2234i	1983i	1865i	1835i	1935i	1832i
ν_2	796	822	790	785	812	783
ν_3	1056	928	930	910	878	859
ν_4	1430	1399	1331	1292	1359	1280
ν_5	2126	1882	1932	1894	1881	1838
ν_6	3276	3243	3193	3245	3145	3140
Largest components of the transition vector						
H–H	−0.90	−0.87	−0.88	−0.85		
C–H_2	0.39	0.39	0.39	0.41		
C–H_1	0.28	0.20	0.22	0.19		

[a]6-31G(d,p) basis, Ref. 28.
[b]6-311G(d,p) basis, present work.
[c]TZ2P basis, Ref. 27.
[d]aVTZ basis, Ref. 22.

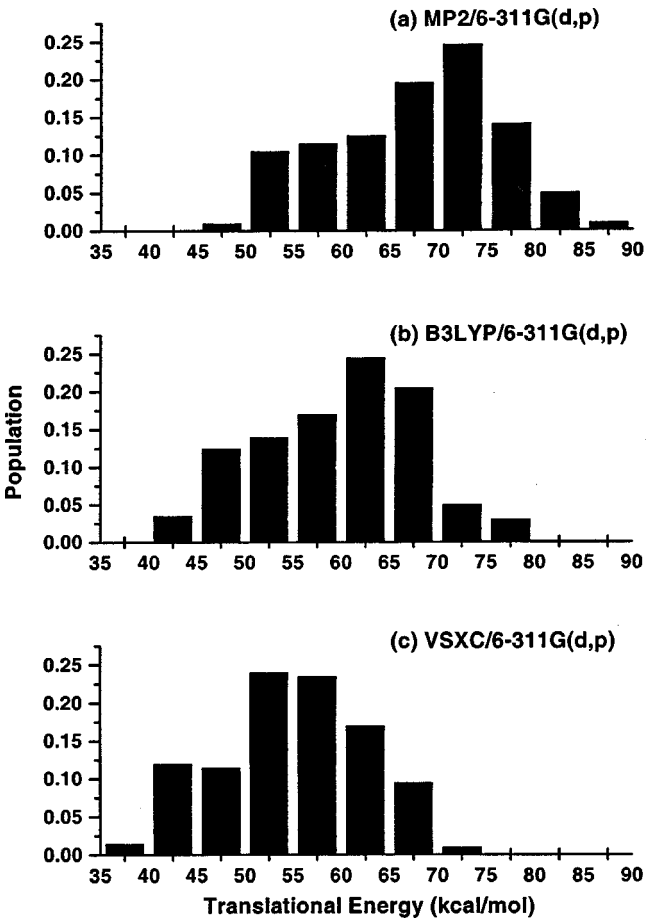

FIG. 3. Translational energy distribution of the photofragments computed at (a) MP2/6-311G(d,p), (b) B3LYP/6-311G(d,p), and (c) VSXC/6-311G(d,p).

TABLE IV. Vibrational energy distribution for the H_2 and CO products.

	CO			H_2					
Level	$v=0$	$v=1$	$\langle v\rangle$	$v=0$	$v=1$	$v=2$	$v=3$	$v=4$	$\langle v\rangle$
HF/3-21G[a]	83.2	16.8	0.17	11.0	30.7	29.5	21.7	6.8	1.82
HF/6-31G(d,p)[a]	82.2	17.8	0.18	22.8	36.5	27.0	11.2	2.5	1.34
MP2/6-311G(d,p)	87.4	12.6	0.13	29.6	34.3	26.6	9.5		1.16
B3LYP/6-311G(d,p)	92.5	7.5	0.07	43.0	33.5	21.0	2.5		0.83
VSXC/6-311G(d,p)	91.9	9.0	0.09	45.5	38.5	14.0	2.0		0.73
EVB/CCSD[b]	88.0	12.0	0.12	25.0	40.0	27.5	7.7		1.18
Experiment[c]	88	12	0.12	24.2	41.3	24.6	8.6	0.3	1.18

[a]Reference 28.
[b]Reference 27.
[c]Reference 6.

tively, compared to ≈0.9 Å experimental[5] and 0.89 for the EVB/CCSD surface.[27] By contrast, the impact parameters obtained from semiempirical trajectory calculations are consistently lower (0.6–0.8 Å).[29] The increase in the impact parameters in going from semiempirical to Hartree–Fock to MP2 and DFT calculations parallels an increase in the H–H distance in the transition state. This may be rationalized using the impulsive model.[8,24]

The vibrational energy distribution of the products is summarized in Table IV. For CO, all of the direct trajectory calculations listed are in very good agreement with experiment,[6] yielding CO primarily in its ground vibrational state with only a small fraction in the first excited state. As was found previously, the population of higher vibrational states of H_2 is greater for $v_{CO}=0$ than for $v_{CO}=1$. All of the calculations listed, except for B3LYP and VSXC, producing H_2 in $v=1$ with the highest population, $v=0$, and $v=2$ with comparable but lower populations and a smaller fraction in $v=3$, in agreement with experiment.[5] Even though the B3LYP and VSXC calculations show considerable vibrational excitation of H_2, the population of $v=0$ is higher than $v=1$, somewhat reminiscent of the semiempirical direct trajectory calculations.[29] The differences between B3LYP and CCSD in the geometry and vibrational frequencies of the transition state are not sufficient to explain the discrepancies in the H_2 vibrational distributions, since the HF transition structures show even larger differences when compared to the CCSD results (see Table I). The variation of the H_2 distance and the projected frequencies along the reaction path also do not offer an explanation since these are essentially superimposable for the four methods considered. However, the variation of the potential energy along the reaction path does provide a possible explanation. Only about half of the potential energy release occurs during the portion of the reaction where most of the changes in the H_2 and CO bond lengths occur. Specifically, by the point that the H_2 bond has completed 80% of the change from the transition state to the products, the potential energy release is 43, 39, 35, 32, and 33 kcal/mol at the HF/3-21G, HF/6-31G(d,p),MP2/6-311G(d,p), B3LYP/6-311G(d,p), and VSXC/6-311G(d,p) levels of theory. Figure 4 shows that this energy release correlates very well with the vibrational excitation of the H_2 as measured by the average quantum number. Thus, the reason that DFT methods do not generate enough vibrationally excited H_2 is because not as much energy is released along the portion of the reaction path where the H_2 bond length changes the most. Likewise, Hartree–Fock produces excess excitation because too much energy is released. Of the semiempirical methods with specific reaction parameters,[29] trajectories with NDDO-SRP5 and -SRP6 reproduce the H_2 vibrational populations quite well, but none of the semiempirical methods yields both the H_2 and CO vibrational energy distributions in agreement with experiment.

The rotational energy distribution of the products appears to be less sensitive to the level of theory than the vibrational distribution. Figure 5 shows that the CO is produced rotationally hot. The average rotational quantum numbers are $\langle J\rangle=43.1$, 46.6, 46.2, 44.4, and 44.7 for HF/3-21G, HF/6-31G(d,p), MP2/6-311G(d,p), B3LYP/6-311G(d,p), and VSXC/6-311G(d,p), respectively, compared to $\langle J\rangle=42$ observed.[6] The distributions are somewhat narrower than experiment (FWHM=14–18 calc. vs 20–22 obs). The trajectories on the EVB/CCSD surface[27] are similar, but the semiempirical direct trajectory calculations yielded significantly lower values ($\langle J\rangle=32$–39).[29] As shown in Fig. 6, the H_2 products are formed with low rota-

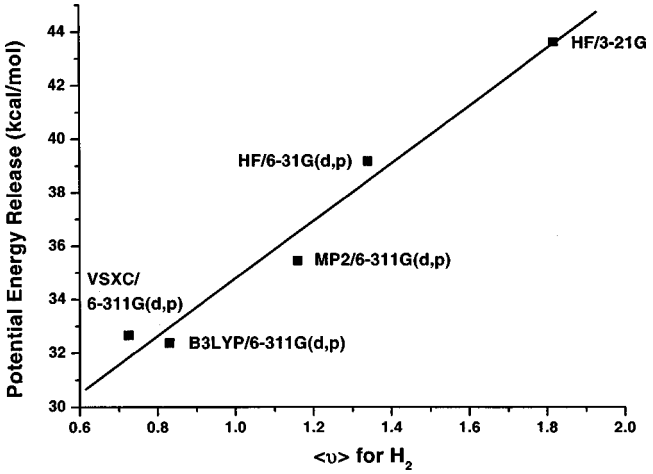

FIG. 4. Comparison of the potential energy release when the H_2 bond has completed 80% of its change from the transition structure to the products with the average quantum number for H_2 vibration in the products at the HF/3-21G, HF/6-31G(d,p), MP2/6-311G(d,p), B3LYP/6-311G(d,p), and VSXC/6-311G(d,p) levels of theory.

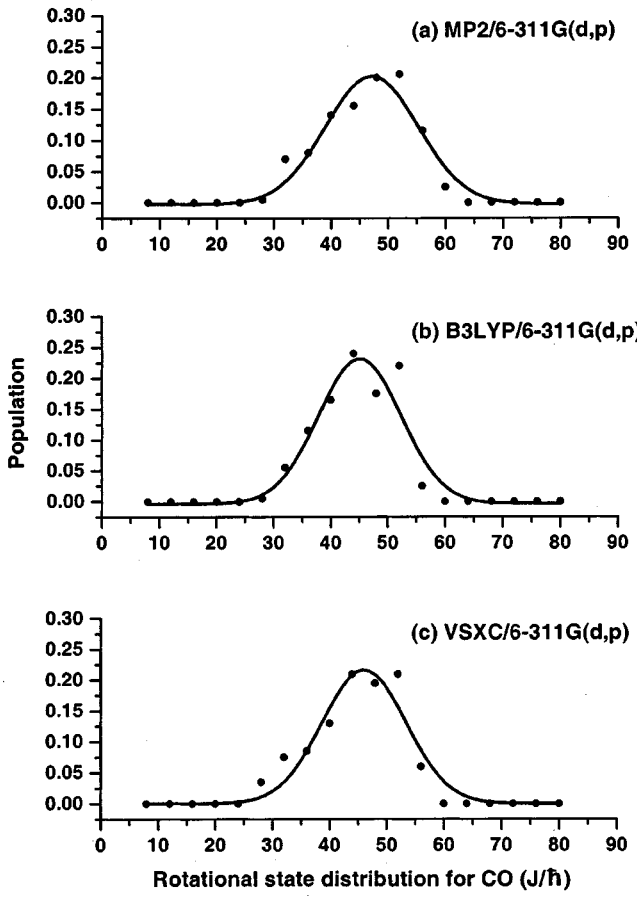

FIG. 5. Rotational state distribution for CO computed at (a) MP2/6-311G(d,p), (b) B3LYP/6-311G(d,p), and (c) VSXC/6-311G(d,p), fitted to a Gaussian.

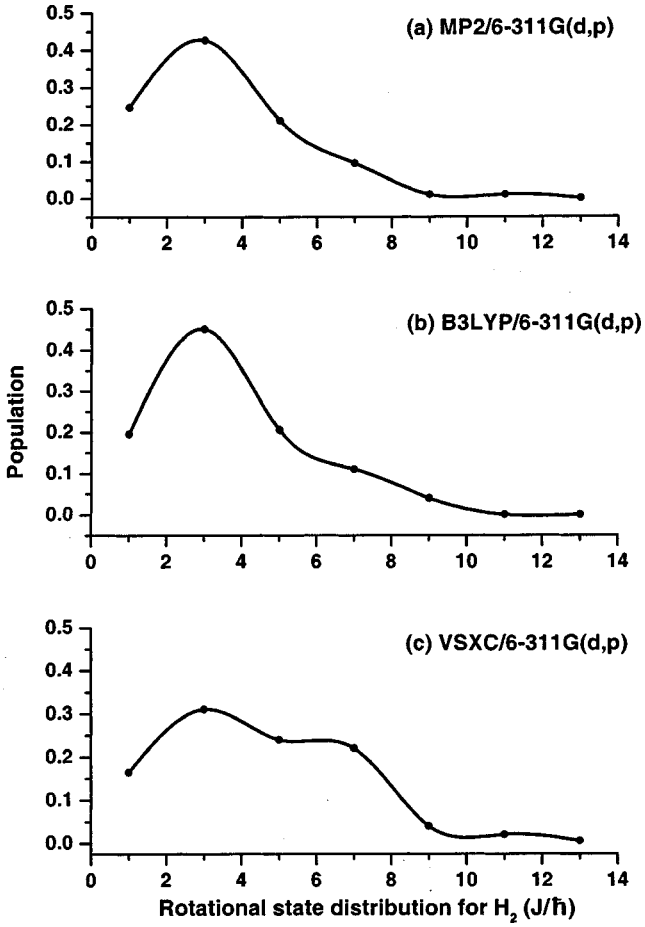

FIG. 6. Rotational state distribution for H_2 computed at (a) MP2/6-311G(d,p), (b) B3LYP/6-311G(d,p), and (c) VSXC/6-311G(d,p).

tional quantum numbers, $\langle J \rangle = 3.2$, 3.1, 3.3, 3.7, and 4.5 for HF/3-21G, HF/6-31G(d,p), MP2/6-311G(d,p), B3LYP/6-311G(d,p), and VSXC/6-311G(d,p), respectively, in agreement with experiment.[5] Neither the H_2 nor the CO rotational distribution shows a strong dependence on the vibrational quantum numbers.

IV. CONCLUSIONS

For direct classical trajectories calculated at the MP2 and DFT levels of theory, the translational energy distribution of the products is in better agreement with experiment than the Hartree–Fock level of theory used in our earlier direct trajectory calculations. This is due to the fact that the MP2 and DFT calculations reproduce the barrier height better than the Hartree–Fock calculations. The MP2 and DFT calculations give very good descriptions of the product rotational state distribution and the CO vibrational state populations, but MP2 yields a better representation of the H_2 vibrational state populations than the DFT or Hartree–Fock methods. This can be traced to the magnitude of the potential energy released along the section of reaction path where the H_2 bond length changes the most.

ACKNOWLEDGMENTS

This work was supported by grants from the National Science Foundation (CHE 9874005 and CISE 9977815). The authors would like to thank William L. Hase for helpful discussions, and Wayne State University for computer time.

[1] P. L. Houston and C. B. Moore, J. Chem. Phys. **65**, 757 (1976).
[2] P. Ho, D. J. Bamford, R. J. Buss, T. T. Lee, and C. B. Moore, J. Chem. Phys. **76**, 3630 (1982).
[3] C. B. Moore and J. C. Weisshaar, Annu. Rev. Phys. Chem. **34**, 525 (1983).
[4] R. D. van Zee, M. F. Foltz, and C. B. Moore, J. Chem. Phys. **99**, 1664 (1993).
[5] D. Debarre, M. Lefrebvre, M. Péalat, and J.-P. E. Taran, J. Chem. Phys. **83**, 4476 (1985).
[6] D. J. Bamford, S. V. Filseth, M. F. Foltz, J. W. Hepburn, and C. B. Moore, J. Chem. Phys. **82**, 3032 (1985).
[7] D. R. Guyer, W. F. Polik, and C. B. Moore, J. Chem. Phys. **84**, 6519 (1986).
[8] T. J. Butenhoff, K. L. Carleton, M. C. Chuang, and C. B. Moore, J. Chem. Soc., Faraday Trans. 2 **85**, 1155 (1989).
[9] W. F. Polik, D. R. Guyer, and C. B. Moore, J. Chem. Phys. **92**, 3453 (1990).
[10] T. J. Butenhoff, K. L. Carleton, and C. B. Moore, J. Chem. Phys. **92**, 377 (1990).
[11] K. L. Carleton, T. J. Butenhoff, and C. B. Moore, J. Chem. Phys. **93**, 3907 (1990).
[12] T. J. Butenhoff, K. L. Carleton, R. D. van Zee, and C. B. Moore, J. Chem. Phys. **94**, 1947 (1991).

[13] R. D. van Zee, C. D. Pibel, T. J. Butenhoff, and C. B. Moore, J. Chem. Phys. **97**, 3235 (1992).
[14] J. D. Goddard and H. F. Schaefer, J. Chem. Phys. **70**, 5117 (1979).
[15] L. B. Harding, H. B. Schlegel, R. Krishnan, and J. A. Pople, J. Phys. Chem. **84**, 3394 (1980).
[16] J. D. Goddard, Y. Yamaguchi, and H. F. Schaefer, J. Chem. Phys. **75**, 3459 (1981).
[17] G. F. Adams, G. D. Bent, R. J. Bartlett, and G. D. Purvis, J. Chem. Phys. **75**, 834 (1981).
[18] M. Dupuis, W. A. Lester, B. H. Lengsfield, and B. Liu, J. Chem. Phys. **79**, 6167 (1983).
[19] M. J. Frisch, J. S. Binkley, and H. F. Schaefer, J. Chem. Phys. **81**, 1882 (1984).
[20] G. E. Scuseria and H. F. Schaefer, J. Chem. Phys. **90**, 3629 (1989).
[21] H. Nakano, K. Nakayama, K. Hirao, and M. Dupuis, J. Chem. Phys. **106**, 4912 (1997).
[22] D. Feller, M. Dupuis, and B. C. Garrett, J. Chem. Phys. **113**, 218 (2000).
[23] J. Troe, J. Phys. Chem. **88**, 4375 (1984).
[24] R. Schinke, Annu. Rev. Phys. Chem. **39**, 39 (1988).
[25] W. H. Miller, R. Hernandez, N. C. Handy, D. Jayatilaka, and A. Willetts, Chem. Phys. Lett. **172**, 62 (1990).
[26] W. L. Hase and K. N. Swamy, Chem. Phys. Lett. **92**, 371 (1982).
[27] Y. T. Chang, C. Minichino, and W. H. Miller, J. Chem. Phys. **96**, 4341 (1992).
[28] W. Chen, W. L. Hase, and H. B. Schlegel, Chem. Phys. Lett. **228**, 436 (1994).
[29] G. H. Peslherbe and W. L. Hase, J. Chem. Phys. **104**, 7882 (1996).
[30] G. C. Schatz, Rev. Mod. Phys. **61**, 669 (1989).
[31] T. Helgaker, E. Uggerud, and H. J. A. Jensen, Chem. Phys. Lett. **173**, 145 (1990).
[32] B. Hartke and E. A. Carter, J. Chem. Phys. **97**, 6569 (1992).
[33] K. Bolton, W. L. Hase, and G. H. Peslherbe, in *Modern Methods for Multidimensional Dynamics Computation in Chemistry*, edited by D. L. Thompson (World Scientific, Singapore, 1998).
[34] C. Møller and M. S. Plesset, Phys. Rev. **46**, 618 (1934).
[35] D. Cremer, in *Encyclopedia of Computational Chemistry*, edited by P. v. R. Schleyer, N. L. Allinger, T. Clark *et al.* (Wiley, Chichester, 1998).
[36] A. D. Becke, Phys. Rev. A **38**, 3098 (1988).
[37] A. D. Becke, J. Chem. Phys. **98**, 5648 (1993).
[38] C. Lee, W. Yang, and R. D. Parr, Phys. Rev. B **37**, 785 (1988).
[39] A. D. Rabuck and G. E. Scuseria, Chem. Phys. Lett. **309**, 450 (1999).
[40] T. Van Voorhis and G. E. Scuseria, J. Chem. Phys. **109**, 400 (1998).
[41] R. Krishnan, J. S. Binkley, R. Seeger, and J. A. Pople, J. Chem. Phys. **72**, 650 (1980).
[42] J. P. Perdew, K. Burke, and Y. Wang, Phys. Rev. B **54**, 16533 (1996).
[43] C. Adamo and V. Barone, Chem. Phys. Lett. **274**, 242 (1997).
[44] J. M. Millam, V. Bakken, W. Chen, W. L. Hase, and H. B. Schlegel, J. Chem. Phys. **111**, 3800 (1999).
[45] V. Bakken, J. M. Millam, and H. B. Schlegel, J. Chem. Phys. **111**, 8773 (1999).
[46] C. Gonzalez and H. B. Schlegel, J. Phys. Chem. **94**, 5523 (1990).
[47] C. Gonzalez and H. B. Schlegel, J. Chem. Phys. **90**, 2154 (1989).
[48] M. J. Frisch, G. W. Trucks, H. B. Schlegel *et al.*, GAUSSIAN 98 (Gaussian, Inc., Pittsburgh, Pennsylvania, 1998).
[49] L. A. Curtiss, K. Raghavachari, G. W. Trucks, and J. A. Pople, J. Chem. Phys. **94**, 7221 (1991).
[50] L. A. Curtiss, J. E. Carpenter, K. Raghavachari, and J. A. Pople, J. Chem. Phys. **96**, 9030 (1992).
[51] K. Raghavachari and L. A. Curtiss, in *Modern Electronic Structure Theory*, edited by D. R. Yarkony (World Scientific, Singapore, 1995), p. 459.
[52] J. A. Montgomery, J. W. Ochterski, and G. A. Petersson, J. Chem. Phys. **101**, 5900 (1994).